JACS
JOURNAL OF THE AMERICAN CHEMICAL SOCIETY
Article
pubs.acs.org/JACS

Synthetic Models for the Active Site of the [FeFe]-Hydrogenase: Catalytic Proton Reduction and the Structure of the Doubly Protonated Intermediate

Maria E. Carroll,[†] Bryan E. Barton,[†] Thomas B. Rauchfuss,*[,†] and Patrick J. Carroll[‡]

[†]School of Chemical Sciences, University of Illinois at Urbana−Champaign, Urbana, Illinois 61801, United States
[‡]Department of Chemistry, University of Pennsylvania, Philadelphia, Pennsylvania 19104, United States

Supporting Information

ABSTRACT: This report compares biomimetic hydrogen evolution reaction catalysts with and without the amine cofactor (adt^{NH}): $Fe_2(adt^{NH})(CO)_2(dppv)_2$ ($\mathbf{1}^{NH}$) and $Fe_2(pdt)(CO)_2(dppv)_2$ (**2**) [$(adt^{NH})^{2-}$ = $HN(CH_2S)_2^{2-}$, pdt^{2-} = 1,3-$(CH_2)_3S_2^{2-}$, and dppv = *cis*-$C_2H_2(PPh_2)_2$]. These compounds are spectroscopically, structurally, and stereodynamically very similar but exhibit very different catalytic properties. Protonation of $\mathbf{1}^{NH}$ and **2** gives three isomeric hydrides each, beginning with the kinetically favored terminal hydride, which converts sequentially to *sym* and *unsym* isomers of the bridging hydrides. In the case of $\mathbf{1}^{NH}$, the corresponding ammonium hydrides are also observed. In the case of the terminal amine hydride [*t*-H$\mathbf{1}^{NH}$]BF_4, the ammonium/amine hydride equilibrium is sensitive to counteranions and solvent. The species [*t*-H$\mathbf{1}^{NH_2}$]$(BF_4)_2$ represents the first example of a crystallographically characterized terminal hydride produced by protonation. The NH---HFe distance of 1.88(7) Å indicates dihydrogen-bonding. The bridging hydrides [μ-H$\mathbf{1}^{NH}$]$^+$ and [μ-H**2**]$^+$ reduce near −1.8 V, about 150 mV more negative than the reductions of the terminal hydride [*t*-H$\mathbf{1}^{NH}$]$^+$ and [*t*-H**2**]$^+$ at −1.65 V. Reductions of the amine hydrides [*t*-H$\mathbf{1}^{NH}$]$^+$ and [*t*-H$\mathbf{1}^{NH_2}$]$^{2+}$ are irreversible. For the pdt analogue, the [*t*-H**2**]$^{+/0}$ couple is unaffected by weak acids (pK_a^{MeCN} = 15.3) but exhibits catalysis with $HBF_4{\cdot}Et_2O$, albeit with a turnover frequency (TOF) around 4 s^{-1} and an overpotential greater than 1 V. The voltammetry of [*t*-H$\mathbf{1}^{NH}$]$^+$ is strongly affected by relatively weak acids and proceeds at 5000 s^{-1} with an overpotential of 0.7 V. The ammonium hydride [*t*-H$\mathbf{1}^{NH_2}$]$^{2+}$ is a faster catalyst, with an estimated TOF of 58 000 s^{-1} and an overpotential of 0.5 V.

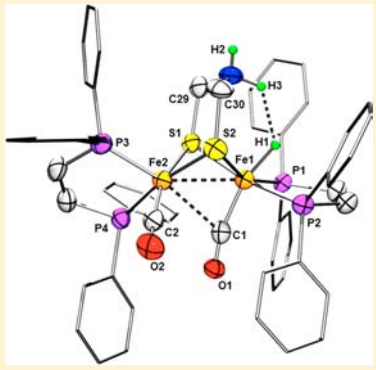

INTRODUCTION

In nature, hydrogen is primarily produced and oxidized by the hydrogenase (H_2ase) enzymes.[1] For example, under fermentative conditions, organisms release accumulated reducing equivalents as H_2. This H_2 can be captured by other organisms, where it is utilized, via hydrogenases, to reduce oxides such as sulfate.[2] These enzymes have attracted attention as proven motifs for the processing of hydrogen.[3,4] A key goal in this area is the elucidation of catalytic mechanisms.

The first step in characterizing a catalytic mechanism is understanding the structure of the active sites. Two genetically unrelated hydrogenases have been identified: they contain Ni and/or Fe thiolate centers, the latter bound to CN^- and CO. These enzymes are generally rich in Fe−S clusters, emphasizing the central role of electron transfer.[5,6] [FeFe]-H_2ases are more active than [NiFe]-H_2ases, and they more commonly function as catalysts for H_2 production (Table 1).[7] In the case of [FeFe]-H_2ases, one 4Fe-4S cluster is directly tethered to the diiron active site; the 6Fe ensemble is called the H-cluster. The [FeFe]-H_2ases also feature an amino-dithiolate cofactor that bridges the two organoiron centers (Figure 1).[8]

One widely embraced method for mechanistic analysis of the enzymes entails studies on synthetic diiron dithiolato compounds that are structurally similar to the active site.[3,9] This approach benefits from many decades of research on organoFe-S clusters.[10] Indeed, soon after the structures of the

Table 1. Activities of [FeFe]- and [NiFe]-Hydrogenases[a,5]

reaction	FeFe	NiFe
H_2 oxidation	28000	700
H_2 production	6000−9000	700

[a]Rates quoted in moles of H_2 per mole of enzyme per second measured at 30 °C.

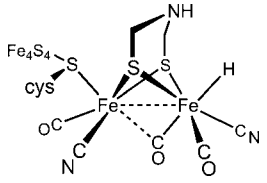

Figure 1. Structure proposed for the active site of [FeFe]-H_2ase in the H_{red} state.[5]

Received: September 17, 2012
Published: November 5, 2012

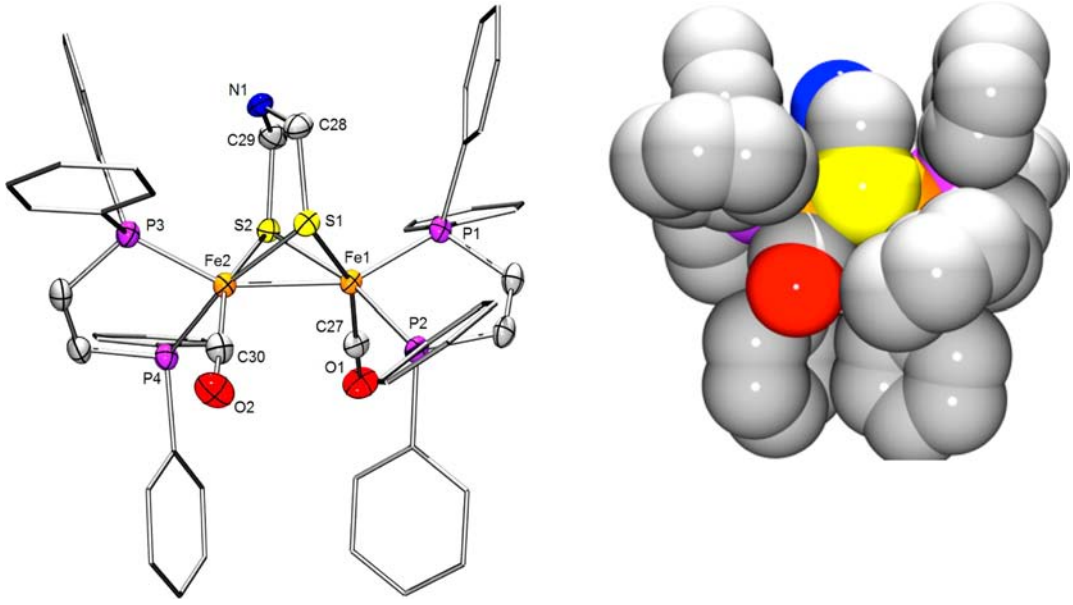

Figure 2. Structure of $Fe_2(adt^{NH})(CO)_2(dppv)_2$. Left: with thermal ellipsoids drawn at the 50% and those for phenyl carbon atoms omitted. Selected distances (Å): Fe1−Fe2, 2.6027(6); Fe1−C27, 1.7381(30); Fe1−P1, 2.1884(8); Fe1−P2, 2.2108(8); Fe1−S1, 2.2108(8); Fe1−S2, 2.2668(8); Fe2−C30, 1.7508(30); Fe2−P3, 2.1937(9); Fe2−P4, 2.2296(8); Fe2−S1, 2.2785(8); Fe2−S2, 2.2668(8). Right: space-filling model showing that the Ph groups block the Fe−Fe bond (red = O, blue = N, yellow = S, orange = Fe, violet = P).

enzymes from *Clostridium pasteurianum* and *Desulfovibrio desulfuricans* were reported, the diiron dithiolato dicyanides $[Fe_2(pdt)(CN)_2(CO)_4]^{2-}$ (pdt = 1,3-propanedithiolate) were described.[11] Unfortunately, these species proved to be not very useful in developing functional models. Since that time, two simplifications have been particularly enabling. First, tertiary phosphine (and other) ligands are used in place of cyanide (and some CO) ligands found in the natural catalysts.[12] Second, in place of the appended 4Fe-4S cluster, models usually rely on electrodes to supply and accept electrons. No compromise is required for the amine-dithiolate cofactor (adt), which is incorporated into our models without modification.[13]

Consensus from biophysical[2] and organometallic[3,12] studies points to the intermediacy of iron hydrides in the catalytic function of [FeFe]-H_2ase. Although much is known about iron hydrides,[14] our understanding of diiron dithiolato hydride frameworks is still underdeveloped. CO-rich compounds such as $Fe_2(SR)_2(CO)_6$ are only protonated by very strong acids,[15] hence the requirement that some CO ligands be replaced by more basic donors. In almost all hydride derivatives of diiron dithiolates, the hydride ligand bridges the two metals. This geometry resembles that found in the [NiFe]-H_2ases, but biophysical[2] and computational studies[16] on the [FeFe]-H_2ases strongly indicate that the hydride is located at the apical position of a single organoFe center. A number of diiron complexes with terminal hydride ligands have been characterized, although usually only by NMR spectroscopy. The terminal hydride complexes $[HFe_2(pdt)(CO)_4(chel)]^+$ (chel = chelating ligand) are often observable by NMR spectroscopy, but above ca. −30 °C they isomerize to bridging hydride complexes.[17,18] The stability of these terminal hydride complexes is enhanced for sterically crowded or very electron-rich diiron dithiolato carbonyls.[19,20] Thus, $Fe_2(pdt)(CO)_2(dppv)_2$ (**2**) [dppv = *cis*-$C_2H_2(PPh_2)_2$] undergoes protonation, albeit only with strong acids, to give a terminal hydride with a half-life of several minutes at room temperature. Additionally, this terminal hydride derivative was shown to reduce at a potential ca. 100 mV less negative than that required for the isomeric bridging hydride complex.[19]

Herein we summarize an extensive investigation of the structural and protonation chemistry of $Fe_2(adt^{NH})(CO)_2(dppv)_2$ ($\mathbf{1}^{NH}$) [$adt^{NH\,2-}$ = $[(SCH_2)_2NH]^{2-}$], with parallel studies on $Fe_2(pdt)(CO)_2(dppv)_2$ (**2**), which lacks the amine cofactor. Overall, the results indicate that the combination of a terminal hydride and the azadithiolate cofactor greatly facilitates reduction of protons to form H_2 by diiron complexes. We also describe a rare crystal structure of a terminal hydride of this series of model diiron dithiolato complexes.

RESULTS

Characterization of $Fe_2(adt^{NH})(CO)_2(dppv)_2$. The main catalyst of interest is $Fe_2(adt^{NH})(CO)_2(dppv)_2$ ($\mathbf{1}^{NH}$), a greenish-brown, air-sensitive solid that is highly soluble in dichloromethane and toluene. The IR spectra for $\mathbf{1}^{NH}$ (ν_{CO} = 1888, 1868 cm^{-1}) and related derivatives $Fe_2(pdt)(CO)_2(dppv)_2$ (**2**), $Fe_2(edt)(CO)_2(dppv)_2$, and $Fe_2(odt)(CO)_2(dppv)_2$ [edt^{2-} = 1,2-$C_2H_4S_2^{2-}$; odt^{2-} = $O(C_2H_4S)_2^{2-}$] are similar, which indicates that they adopt similar structures and that the donor properties of the dithiolates are similar.[21] Compounds $\mathbf{1}^{NH}$ and **2** are stereochemically nonrigid in two ways: (i) "turnstile rotation" of the Fe(dppv)(CO) subunits and (ii) "flipping" of the dithiolate bridge. With respect to the latter process, the $X(CH_2S)_2Fe$ rings (X = CH_2, NH, O, etc.) are subject to a chair−chair equilibration,[22] as seen in cyclohexane and piperidine derivatives.[23]

At −80 °C, the ^{31}P NMR spectrum of $\mathbf{1}^{NH}$ displays four equally intense signals, indicating that the two dppv ligands are chemically inequivalent. In contrast, spectra for the related pdt complexes show only a pair of signals at low temperatures, an observation that suggests that pdt^{2-} is a more flexible dithiolate than adt^{2-}. In the pdt derivative, turnstile rotation at the Fe(dppv)(CO) unit is halted on the NMR time scale at −80 °C, but flipping of the dithiolate remains fast. In the adt

dx.doi.org/10.1021/ja309216v | J. Am. Chem. Soc. 2012, 134, 18843−18852

derivative, both processes are either slow or cease to occur at low temperatures, which may reflect a higher barrier for the flipping of the adt compared to the structurally related pdt derivative. [Note: The barriers for ring flipping for the $Fe_2(xdt)(CO)_4(dppv)$ [xdt^{2-} = pdt, odt, and adt] from DNMR studies (at coalescence temperatures, K) are as follow: pdt, 42 (225); odt, 43.3 (235); and adt, 55.9 kJ/mol (293). The variation reflects increased stiffness of the two C−N bonds in the adt backbone, as a consequence of the interaction of the amine lone pair and the C−S σ^* orbitals. M. T. Olsen, unpublished results.] At −10 °C, this conformational equilibrium becomes rapid on the NMR time scale, and the ^{31}P NMR spectrum simplifies to a broad singlet. The dynamics of the adt and the turnstile rotation of the Fe(CO)(dppv) centers appear to be coupled since both processes change from slow to fast exchange regimes at the same temperature range (see Supporting Information (SI)).

The structure of $\mathbf{1}^{NH}$ was confirmed crystallographically (Figure 2), the details being consistent with the NMR results. Space-filling models show that the phenyl groups protect the Fe−Fe bond, which is relevant to the regiochemistry of the protonation of $\mathbf{1}^{NH}$ and **2**.

Protonated Derivatives of $Fe_2(adt^{NH})(CO)_2(dppv)_2$. Protonation of $\mathbf{1}^{NH}$ gives three isomeric hydrides as well as ammonium derivatives or combinations of both. Addition of $[H(OEt_2)_2]BAr^F{}_4$ to a CH_2Cl_2 solution of $\mathbf{1}^{NH}$ at −80 °C initially afforded the terminal hydride $[t\text{-}HFe_2(adt^{NH})(CO)_2(dppv)_2]^+$ ($[t\text{-}H\mathbf{1}^{NH}]^+$) ($BAr^F{}_4^-$ = $B(3,5\text{-}C_6H_3(CF_3)_2)_4^-$, Scheme 1). Its high-field ^1H NMR spectrum,

Scheme 1. Protonation of $\mathbf{1}^{NH}$ and Isomerization Reactions of the Resulting Hydrides

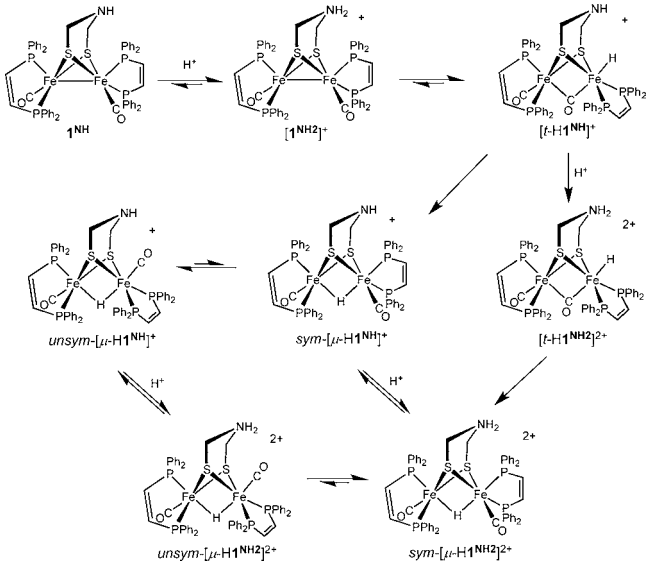

a triplet near δ −4.2, indicates a single isomer (Table 2, Figure 3). Such relatively low field chemical shifts are often associated with terminal hydrides of diiron dithiolates.[17−20] The ^{31}P NMR spectrum, which features four equally intense singlets (Table 2), uniquely defines the stereochemistry at the diiron center: the diphosphine on the FeH center is dibasal and the diphosphine on the other ("proximal") Fe center spans apical and basal sites ($^{31}P-^{31}P$ coupling is often weak in such complexes).[24]

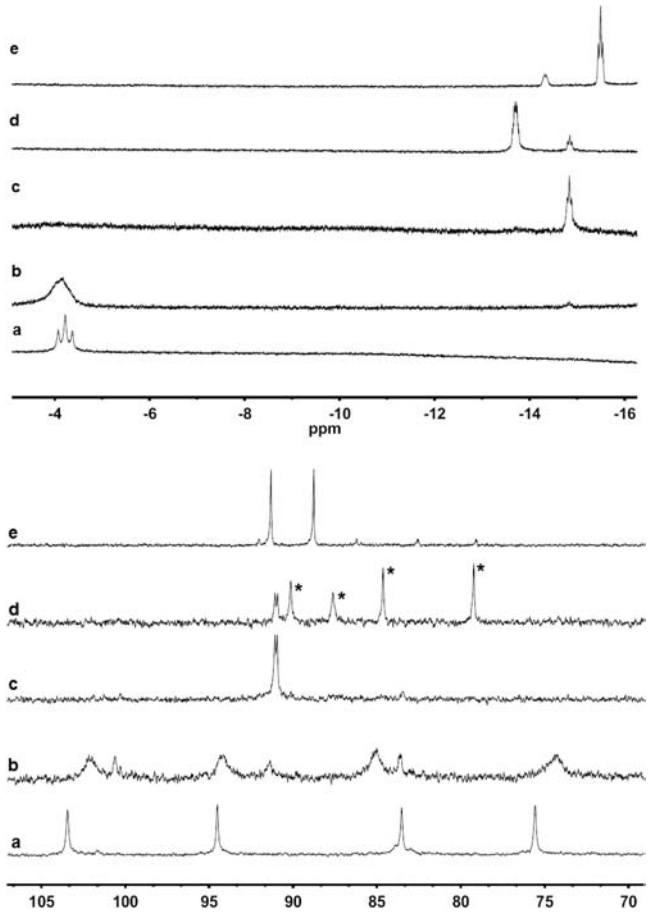

Figure 3. (Top) ^1H and (bottom) ^{31}P NMR spectra of the protonation of $\mathbf{1}^{NH}$ with $[H(OEt_2)_2]BAr^F{}_4$ in CD_2Cl_2 at various times and temperatures. Spectra a: −80 °C ($[t\text{-}H\mathbf{1}^{NH}]^+$). Spectra b: sample warmed to −10 °C. Spectra c: sample warmed to 20 °C (*sym*-$[\mu\text{-}H\mathbf{1}^{NH}]^+$; this spectrum does not change upon recooling to 0 °C). Spectra d: previous sample after standing at 20 °C for 24 h (*sym*- and *unsym*-$[\mu\text{-}H\mathbf{1}^{NH}]^+$, the latter indicated by asterisks). Spectra e: same sample after addition of 1 equiv of $[H(OEt_2)_2]BAr^F{}_4$ (mainly *sym*-$[\mu\text{-}H\mathbf{1}^{NH_2}]^{2+}$ and a small amount of the *unsym* isomer).

The NMR spectrum of $[t\text{-}H\mathbf{1}^{NH}]^+$ changes at higher temperatures. Above −20 °C, the triplet at δ −4.2 in the ^1H NMR spectrum broadens, as do the ^{31}P NMR signals, consistent with exchange between the hydride and ammonium tautomers (Scheme 2). Near room temperature, $[t\text{-}H\mathbf{1}^{NH}]^+$ converts sequentially to two isomers that feature bridging hydride ligands ("μ-hydrides", Scheme 1). The first μ-hydride isomer, *sym*-$[\mu\text{-}H\mathbf{1}^{NH}]^+$, has C_2-symmetry (ignoring the adt ligand, which is rapidly flexing and hence effectively planar). In *sym*-$[\mu\text{-}H\mathbf{1}^{NH}]^+$, each dppv ligand spans one apical and one basal site. Upon recooling a solution of *sym*-$[\mu\text{-}H\mathbf{1}^{NH}]^+$ to 0 °C, the terminal hydride species does not re-form. Within minutes at room temperature, *sym*-$[\mu\text{-}H\mathbf{1}^{NH}]^+$ converts to an unsymmetrical isomer labeled *unsym*-$[\mu\text{-}H\mathbf{1}^{NH}]^+$. In *unsym*-$[\mu\text{-}H\mathbf{1}^{NH}]^+$, one diphosphine remains apical-basal and the other is dibasal as indicated by the ^{31}P NMR spectrum, which consists of four singlets. After the solution was allowed to stand for 12 h at room temperature, a 1:5 equilibrium distribution was reached, favoring *unsym*-$[\mu\text{-}H\mathbf{1}^{NH}]^+$. The isomerization of ($[t\text{-}H\mathbf{1}^{NH}]^+$ is similar to that observed for the hydrides of **2**.[18]

Addition of $[H(OEt_2)_2]BAr^F{}_4$ to a CH_2Cl_2 solution of $[\mu\text{-}H\mathbf{1}^{NH}]^+$ shifts the ν_{CO} pattern about 15 cm^{-1} to higher energy.

dx.doi.org/10.1021/ja309216v | J. Am. Chem. Soc. 2012, 134, 18843−18852

Table 2. Spectroscopic Properties for 1^{NH}, 2, and Their Protonated Derivatives in CD_2Cl_2 Solution

complex	IR: ν_{CO} (cm^{-1})	^1H NMR: δ hydride (ppm)	^{31}P NMR (ppm)
$Fe_2(adt^{NH})(CO)_2(dppv)_2$, $\mathbf{1}^{NH}$	1888, 1868		91.2; at −70 °C: 102.6, 93.4, 92.2, 88.6
$[t\text{-}HFe_2(adt^{NH})(CO)_2(dppv)_2]^+$, $[t\text{-}H\mathbf{1}^{NH}]^+$	1965, 1915	−4.2 (t), J = 73 Hz	103.2, 94.5, 84.0, 75.1
$[t\text{-}HFe_2(adt^{NH_2})(CO)_2(dppv)_2]^{2+}$, $[t\text{-}H\mathbf{1}^{NH_2}]^{2+}$	1986, 1925	−4.95 (t), J = 72 Hz	98, 89, 76, 74
$[Fe_2(adt^{NH})(\mu\text{-}H)(CO)_2(dppv)_2]^+$, *sym*-$[\mu\text{-}H\mathbf{1}^{NH}]^+$	not obsvd	−14.8 (tt) J = 25, 5 Hz	91.1, 90.9
$[Fe_2(adt^{NH})(\mu\text{-}H)(CO)_2(dppv)_2]^+$, *unsym*-$[\mu\text{-}H\mathbf{1}^{NH}]^+$	1948, 1969	−13.7 (dtd)	90.1, 87.6, 84.6, 79.2
$[Fe_2(adt^{NH_2})(\mu\text{-}H)(CO)_2(dppv)_2]^{2+}$, *sym*-$[\mu\text{-}H\mathbf{1}^{NH_2}]^{2+}$	1967, 1985	−15.6 (tt), J = 20, 5 Hz	91.3, 88.7
$[Fe_2(adt^{NH_2})(\mu\text{-}H)(CO)_2(dppv)_2]^{2+}$, *unsym*-$[\mu\text{-}H\mathbf{1}^{NH_2}]^{2+}$	not obsvd	−14.5 (dtd)	92.3, 86.0, 82.4, 79.0
$Fe_2(pdt)(CO)_2(dppv)_2$, **2**	1888, 1868		90.8; at −80 °C: 97, 88.5
$[HFe_2(pdt)(CO)_2(dppv)_2]^+$, $[t\text{-}H\mathbf{2}]^+$	1965, 1905	−3.5 (t), J = 78 Hz	99, 91, 86, 68
$[Fe_2(pdt)(\mu\text{-}H)(CO)_2(dppv)_2]^+$, *sym*-$[\mu\text{-}H\mathbf{2}]^+$	not obsvd	−15.6 (tt), J = 24, 6 Hz	89.6, 89.4
$[Fe_2(pdt)(\mu\text{-}H)(CO)_2(dppv)_2]^+$, *unsym*-$[\mu\text{-}H\mathbf{2}]^+$	1951, 1968	−14.5 (dddd), J = 24, 19, 19, 10 Hz	76.7, 82.7, 84.2, 87.9

Scheme 2. Proposed Hydrogen-Bonding Interaction between $[\mathbf{1}^{NH_2}]^+$ and BF_4^- Resulting in Stabilization of the Ammonium Tautomer

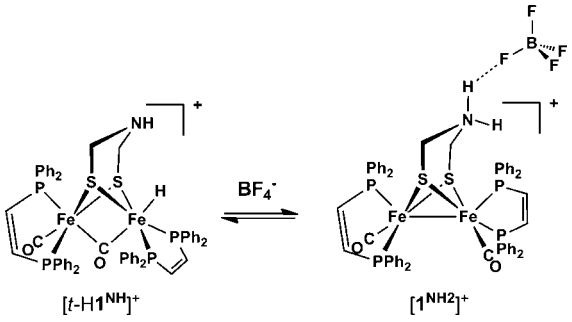

This change is indicative of *N*-protonation to form the ammonium hydride $[\mu\text{-}H\mathbf{1}^{NH_2}]^{2+}$ (Scheme 1).[25] *N*-Protonation is also indicated by the ^1H NMR signal for the hydride, which shifts to higher field. The symmetrical isomer, *sym*-$[\mu\text{-}H\mathbf{1}^{NH_2}]^{2+}$, is the major species in solution, in contrast to the situation for $[\mu\text{-}H\mathbf{2}]^+$ and $[\mu\text{-}H\mathbf{1}^{NH}]^+$.

IR spectroscopic measurements on the protonation reactions are consistent with the sequence of reactions proposed in Scheme 1. The main feature of interest is the ca. 70 cm^{-1} shift in $\nu_{CO,avg}$ upon protonation of $\mathbf{1}^{NH}$ by $[H(OEt_2)_2]BAr^F{}_4$. IR spectra in the ν_{CO} region also distinguish terminal and bridging hydrides. The terminal hydrides shows two well-resolved bands, ν_{CO} = 1965 and 1915 cm^{-1}, with the band at lower frequency assigned to the semibridging CO (Figure 4). The IR spectra of μ-hydrides show two bands, $\nu_{CO} \approx$ 1948 and 1969 cm^{-1}.

Protonation of $Fe_2(adt^{NH})(CO)_2(dppv)_2$ with $HBF_4{\cdot}Et_2O$. The identity of the acid affects the course of protonation of $\mathbf{1}^{NH}$. Thus, treatment of CH_2Cl_2 solutions with $HBF_4{\cdot}Et_2O$ (vs $[H(OEt_2)_2]BAr^F{}_4$ discussed above) afforded not only $[t\text{-}H\mathbf{1}^{NH}]^+$ but also a second species. The pattern for the ν_{CO} bands for the other species is identical to that for $\mathbf{1}^{NH}$, but the bands are shifted approximately 20 cm^{-1} to higher energy, characteristic of *N*-protonation (Figure 4).[25,26] The new species is thus assigned as the ammonium tautomer ($[\mathbf{1}^{NH_2}]^+$, Schemes 1 and 2). The formation of the tautomer is attributed to the ability of BF_4^- to participate in hydrogen-bonding (Scheme 2),[27] which has been observed previously in complexes of protonated adt ligands.[28] The ratio $[t\text{-}H\mathbf{1}^{NH}]^+/[\mathbf{1}^{NH_2}]^+$ increased from 2:1 to approximately 1:1 in the presence of 10 equiv of $[Bu_4N]BF_4$. Although BF_4^- stabilizes the ammonium tautomer, the mixture isomerizes in the usual way, forming the μ-hydride species over the course of minutes at room temperature.

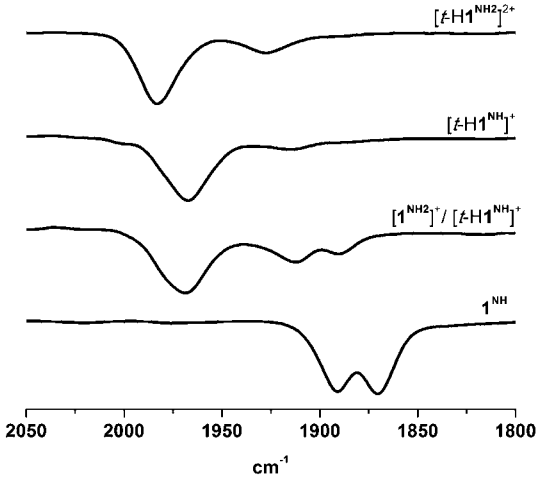

Figure 4. FT-IR spectra in the ν_{CO} region of $\mathbf{1}^{NH}$ (bottom) and products from its protonation in CH_2Cl_2. A mixture of the ammonium cation $[\mathbf{1}^{NH_2}]^+$ and $[t\text{-}H\mathbf{1}^{NH}]^+$ generated by addition of excess $[Bu_4N]BF_4$ to a solution of $[t\text{-}H\mathbf{1}^{NH}]^+$. The terminal hydride, $[t\text{-}H\mathbf{1}^{NH}]^+$, formed by protonation of **1** with 1 equiv of $[H(OEt_2)_2]BAr^F{}_4$ at −40 °C. The terminal hydride ammonium dication $[t\text{-}H\mathbf{1}^{NH_2}]^{2+}$ formed by protonation of $\mathbf{1}^{NH}$ with 2 equiv of $HBF_4{\cdot}Et_2O$ at −40 °C.

Diprotonation of $Fe_2(adt^{NH})(CO)_2(dppv)_2$. Relevant to the electrocatalysis discussed below, $\mathbf{1}^{NH}$ undergoes double protonation. Addition of *excess* of $[H(OEt_2)_2]BAr^F{}_4$, $HBF_4{\cdot}Et_2O$, or CF_3CO_2H to a CH_2Cl_2 solution of $[t\text{-}H\mathbf{1}^{NH}]^+$ gave a new species assigned as the ammonium hydride $[t\text{-}H\mathbf{1}^{NH_2}]^{2+}$ (Figures 3 and 4). According to ^1H and ^{31}P NMR spectra, $[t\text{-}H\mathbf{1}^{NH_2}]^{2+}$ is structurally similar to $[t\text{-}H\mathbf{1}^{NH}]^+$, i.e., a single isomer with both dibasal and apical-basal diphosphine ligands (Table 2, Scheme 1). As seen for $\mathbf{1}^{NH}$ vs $[\mathbf{1}^{NH_2}]^+$, *N*-protonation shifts ν_{CO} bands to higher energy by 20 cm^{-1}, compared to that for $[t\text{-}H\mathbf{1}^{NH}]^+$.

After attempts over the course of several years, single crystals of an ammonium hydride were obtained in the form of the salt $[t\text{-}H\mathbf{1}^{NH_2}](BF_4)_2$ (Figure 5). In the dication, two Fe(dppv)-(CO) centers are linked in the usual way by a dithiolate. One CO ligand is semibridging with Fe−Fe−C and Fe−C−O angles of 66.68(14) and 166.1(4)°, respectively.[29] The dispositions of the dppv groups, being dibasal and apical-basal, conform with the NMR measurements. The crystals are of sufficient quality that the H centers attached to nitrogen and iron were located and refined. Two phenyl groups on the Fe(1)(dppv) center, equivalent to the distal Fe in the active site, form a pocket around the Fe−H and N−H centers. The Fe−H distance of 1.44(4) Å is normal for a ferrous hydride.[30] The ammonium

dx.doi.org/10.1021/ja309216v | J. Am. Chem. Soc. 2012, 134, 18843−18852

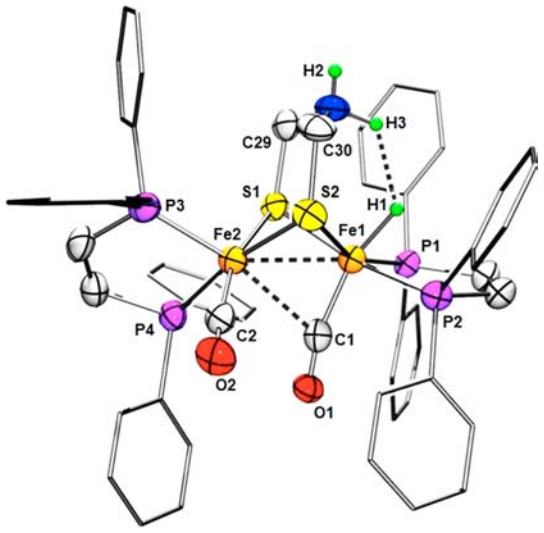

Figure 5. Structure of $[t\text{-HFe}_2(\text{adt}^{\text{NH}_2})(\text{CO})_2(\text{dppv})_2](\text{BF}_4)_2$ with thermal ellipsoids drawn at 50% probability and those for phenyl carbon atoms omitted for clarity. Counterions and solvent of crystallization are not shown. Selected distances (Å): H1---H2, 1.88(7); Fe1−C1, 1.794(5); Fe1−P2, 2.2141(13); Fe1−P1, 2.2196(12); Fe1−S2, 2.2610(12); Fe1−S1, 2.3009(13); Fe1−Fe2, 2.6155(9); Fe1−H1, 1.44(4); Fe2−C2, 1.769(5); Fe2−P3, 2.2122(14); Fe2−S2, 2.2348(14); Fe2−S1, 2.2564(12); Fe2−P4, 2.2686(14). Angles (°): C1−Fe1−Fe2, 66.68(14); Fe2−Fe1−H1, 130.3(18); S2−Fe1−S1, 83.50(4); S2−Fe2−S1, 85.12(4); O1−C1−Fe1, 166.1(4).

center of the dithiolate cofactor adtH^+ is adjacent to the Fe-*H* center. The NH---HFe distance of 1.88(7) Å is shorter than 2.4 Å distance that is twice the van der Waals radius of hydrogen,[31] indicative of dihydrogen-bonding.

Protonation of $Fe_2(xdt)(CO)_2(dppv)_2$ [xdt = adt^{NH}, pdt] with Weak Acids. In this section we discuss protonations using acids with pK_a^{MeCN} between 12 and 19. Weak acids that do not convert $\mathbf{1}^{\mathbf{NH}}$ into detectable levels of $[t\text{-H}\mathbf{1}^{\mathbf{NH}}]^+$ at low temperatures quantitatively give $[\mu\text{-H}\mathbf{1}^{\mathbf{NH}}]^+$ near room temperature. Thus, $[\text{HNMe}_3]\text{BAr}^{\text{F}}{}_4$ (pK_a^{MeCN} = 17.6)[32] rapidly converted **1** to $[\mu\text{-H}\mathbf{1}^{\mathbf{NH}}]^+$, whereas the same reaction using $[\text{HNEt}_3]\text{BF}_4$ (pK_a^{MeCN} = 18.6)[32] required days for 50% conversion.

Addition of >2 equiv of $\text{CF}_3\text{CO}_2\text{H}$ (pK_a^{MeCN} = 12.7)[32] to $\mathbf{1}^{\mathbf{NH}}$ at −40 °C gave $[t\text{-H}\mathbf{1}^{\mathbf{NH_2}}]^{2+}$. The IR spectrum ($\nu_{CO}$ = 1986 and 1950 cm^{-1}) of the trifluoroacetate differs from that (ν_{CO} = 1986 and 1925 cm^{-1}) obtained by protonation with $[\text{H}(\text{OEt}_2)_2]\text{BAr}^{\text{F}}{}_4$ and $\text{HBF}_4\cdot\text{Et}_2\text{O}$, a difference tentatively attributed to hydrogen-bonding between the trifluoroacetate and the protonated adt ligand. In contrast to the acid−base behavior of $\mathbf{1}^{\mathbf{NH}}$, the pdt derivative, **2**, is unaffected by weak acids.

Redox Properties of the Protonated Derivatives of $Fe_2(xdt)(CO)_2(dppv)_2$ [xdt = adt^{NH}, pdt]. In CH_2Cl_2 solutions, the μ-hydrides $[\mu\text{-H}\mathbf{1}^{\mathbf{NH}}]^+$ and $[\mu\text{-H}\mathbf{2}]^+$ reversibly reduce near −1.8 V. Reduction of the doubly protonated species $[\mu\text{-H}\mathbf{1}^{\mathbf{NH_2}}]^{2+}$ occurs about 100 mV positive of the $[\mu\text{-H}\mathbf{1}^{\mathbf{NH}}]^{+/0}$ couple, as observed for other adt-hydrido complexes.[33] The terminal hydrides $[t\text{-H}\mathbf{1}^{\mathbf{NH}}]^+$ and $[t\text{-H}\mathbf{2}]^+$ are redox-active at milder potentials, the pdt derivative $[t\text{-H}\mathbf{2}]^+$ reducing quasi-reversibly (i_{pa}/i_{pc} = 1.57) at −1.67 V. Reduction of $[t\text{-H}\mathbf{2}]^+$ is a $1e^-$ process, as indicated by the similarity of the dependence of i_p vs $\nu^{1/2}$ for the couples $[t\text{-H}\mathbf{2}]^{+/0}$ and $[\mathbf{2}]^{0/+}$.[19] We have independently established the stoichiometry of the $[\mathbf{2}]^{0/+}$ couple.[34] The amino hydride $[t\text{-H}\mathbf{1}^{\mathbf{NH}}]^+$ reduces at nearly the same potential (−1.64 V), but the couple is *irreversible*, in contrast to the $[t\text{-}\mathbf{2}\text{H}]^{+/0}$ couple. The ammonium hydride $[t\text{-H}\mathbf{1}^{\mathbf{NH_2}}]^{2+}$ also reduces irreversibly but at the mild potential of −1.3 V (Table 3). Although the reduction potential is milder, stronger acids are required to generate this doubly protonated species. Finally, both the $[t\text{-H}\mathbf{1}^{\mathbf{NH}}]^{+/0}$ and the $[t\text{-H}\mathbf{2}]^{+/0}$ couples proved insensitive to the electrolyte, i.e., $[\text{Bu}_4\text{N}]\text{BAr}^{\text{F}}{}_4$ and $[\text{Bu}_4\text{N}]\text{PF}_6$.

Proton Reduction Catalysis by $Fe_2(pdt)(CO)_2(dppv)_2$. For comparison with the catalyst that contains the amine cofactor, the catalytic properties of $[t\text{-H}\mathbf{2}]^+$ and $[\mu\text{-H}\mathbf{2}]^+$ were evaluated. Strong acids such $\text{HBF}_4\cdot\text{Et}_2\text{O}$ (pK_a^{MeCN} = −3)[35] are required to protonate **2**, readily giving the terminal hydride $[t\text{-H}\mathbf{2}]^+$, which is stable for many minutes at 0 °C. The $[t\text{-H}\mathbf{2}]^{+/0}$ couple at −1.67 V is partially reversible even at scan rates as slow as 25 mV/s. Addition of $\text{ClCH}_2\text{CO}_2\text{H}$ (pK_a^{MeCN} = 15.3)[35] has no effect on the electrochemical properties of $[t\text{-H}\mathbf{2}]^+$. Addition of $\text{HBF}_4\cdot\text{Et}_2\text{O}$ results in an increase in current for the couple at −1.67 V, indicative of catalysis. The ratio of the catalytic current to the peak current in the absence of excess acid, i_c/i_p, increases linearly with $[\text{H}^+]$ up to 8 equiv of acid, indicating a catalytic pathway that is second order with respect to $[\text{H}^+]$. Above this level, i_c/i_p reaches a plateau near 5. The turnover frequency (TOF) is calculated to be ∼5 s^{-1} (see SI). The overpotential is estimated to be 1.3 V. Overpotentials represent the difference between the catalytic potential, E_{cat}, and the standard reduction potential of the acid, $E^\circ_{HA/H2}$ (see Table 4).

The catalytic properties of $[\mu\text{-}\mathbf{2}\text{H}]^+$ were also examined. Addition of $\text{ClCH}_2\text{CO}_2\text{H}$ to a solution of $[\mu\text{-}\mathbf{2}\text{H}]\text{BF}_4$ results in an increase in the current for the −1.8 V couple (see SI). Plots of i_c/i_p vs $[\text{H}^+]$ are linear up to 10 equiv of acid, and the rate of catalysis by this derivative is calculated to be ∼3 s^{-1}. The overpotential is estimated to be 0.95 V for this very slow process.[35]

Table 3. Selected Electrochemical Properties of 1 and 2 and Their Protonated Derivatives[a]

complex	$E_{1/2}$ in CH_2Cl_2 (V vs $\text{Fc}^{+/0}$)	assignment	i_{pc}/i_{pa}
$[t\text{-HFe}_2(\text{adt}^{\text{NH}})(\text{CO})_2(\text{dppv})_2]^+$, $[t\text{-H}\mathbf{1}^{\mathbf{NH}}]^+$	−1.64	$[t\text{-H}\mathbf{1}^{\mathbf{NH}}]^{+/0}$	*b*
$[t\text{-HFe}_2(\text{adt}^{\text{NH}_2})(\text{CO})_2(\text{dppv})_2]^{2+}$, $[t\text{-H}\mathbf{1}^{\mathbf{NH_2}}]^{2+}$	−1.4	$[t\text{-H}\mathbf{1}^{\mathbf{NH_2}}]^{2+/+}$	*b*
$[\text{Fe}_2(\text{adt}^{\text{NH}})(\mu\text{-H})(\text{CO})_2(\text{dppv})_2]^+$, $[\mu\text{-H}\mathbf{1}^{\mathbf{NH}}]^+$	−1.86	$[\mu\text{-H}\mathbf{1}^{\mathbf{NH}}]^{+/0}$	1.19
$[\text{Fe}_2(\text{adt}^{\text{NH}_2})(\mu\text{-H})(\text{CO})_2(\text{dppv})_2]^{2+}$, $[\mu\text{-H}\mathbf{1}^{\mathbf{NH_2}}]^{2+}$	−1.77	$[\mu\text{-H}\mathbf{1}^{\mathbf{NH_2}}]^{2+/+}$	1.00
$[\text{HFe}_2(\text{pdt})(\text{CO})_2(\text{dppv})_2]^+$, $[t\text{-H}\mathbf{2}]^+$	−1.67	$[t\text{-H}\mathbf{2}]^{+/0}$	1.57
$[\text{Fe}_2(\text{pdt})(\mu\text{-H})(\text{CO})_2(\text{dppv})_2]^+$, $[\mu\text{-H}\mathbf{2}]^+$	−1.8	$[\mu\text{-H}\mathbf{2}]^{+/0}$	1.07

[a]Electrolytes for measurements: $[\text{Bu}_4\text{N}]\text{BAr}^{\text{F}}{}_4$ (for **1**) and $[\text{Bu}_4\text{N}]\text{PF}_6$ (for **2**). [b]Irreversible.

Table 4. Selected Electrocatalytic Properties of Protonated Derivatives of 1 and 2

catalyst	acid	equiv of H^+ linear region	equiv of H^+ plateau region	$(i_c/i_p)_{max}$ [a]	k (s^{-1})	E_{cat} [b] (V vs $Fc^{+/0}$)	overpotential [c] (V)
$[HFe_2(adt^{NH})(CO)_2(dppv)_2]^+$, $[t\text{-}H\mathbf{1}^{NH}]^+$	$ClCH_2CO_2H$	50–400	600–1200	69	5000	−1.49	0.71
$[HFe_2(adt^{NH}H)(CO)_2(dppv)_2]^{2+}$, $[t\text{-}H\mathbf{1}^{NH_2}]^{2+}$	CF_3CO_2H	40–560	740–1300	167	58000	−1.11	0.51
$[Fe_2(adt^{NH})(\mu\text{-}H)(CO)_2(dppv)_2^+$, $[\mu\text{-}H\mathbf{1}^{NH}]^+$	$ClCH_2CO_2H$	2–50	60–90	10	20	−1.72	0.90
$[HFe_2(pdt)(CO)_2(dppv)_2]^+$, $[t\text{-}H\mathbf{2}]^+$	$HBF_4{\cdot}Et_2O$	1–8	10–20	5	5	−1.49	1.32
$[Fe_2(pdt)(\mu\text{-}H)(CO)_2(dppv)_2]^+$, $[\mu\text{-}H\mathbf{2}]^+$	$ClCH_2CO_2H$	2–10	14–40	3.5	3	−1.78	0.95

[a] i_c is the average catalytic current in the plateau region [b] E_{cat} was calculated at each acid concentration in the linear region by the method described by Fourmond et al.,[37] considering the effects of homoconjugation for the two carboxylic acids. The values listed are averages from each acid concentration in the linear region. [c] Overpotential = $E^\circ_{HA/H2} - E_{cat}$, where $E^\circ_{HA/H2}$ is the standard reduction potential of the acid.[37]

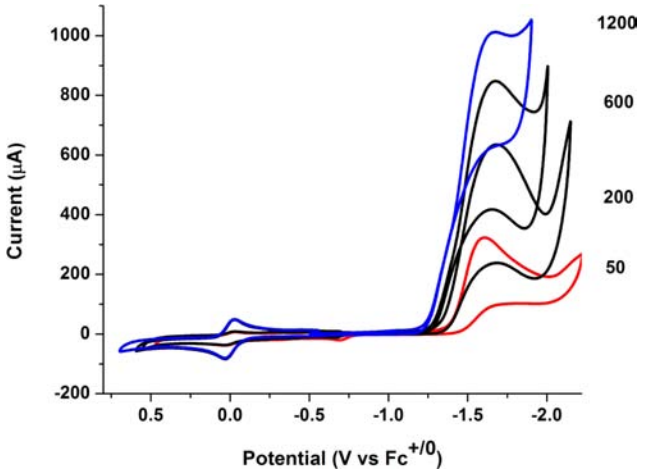

Figure 6. Cyclic voltammograms of a 1.00 mM solution of $\mathbf{1}^{NH}$ (0 °C, 0.125 M $[Bu_4N]BAr^F_4$, CH_2Cl_2, scan rate = 0.5 V/s, glassy carbon working electrode, Pt counter electrode, Ag wire pseudo reference electrode, Fc internal standard) recorded with increasing equivalents of $ClCH_2CO_2H$ (shown to right of voltammograms).

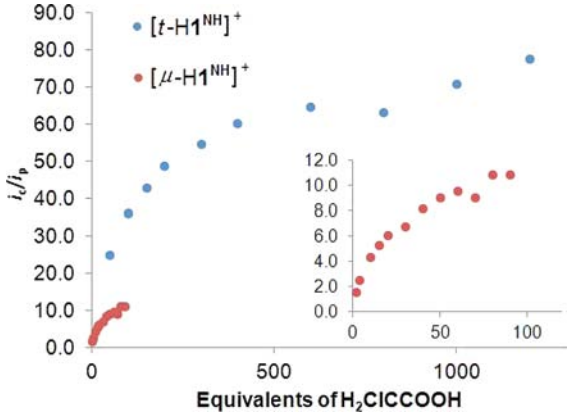

Figure 7. Graph of i_c/i_p vs equivalents of acid for the addition of $ClCH_2CO_2H$ to a 1.00 mM solution of $\mathbf{1}^{NH}$ with $[Bu_4N]BAr^F_4$ as supporting electrolyte (blue) and a 1.0 M solution of $[\mu\text{-}H\mathbf{1}^{NH}]^+$ with $[Bu_4N]PF_6$ as supporting electrolyte (red). Inset: magnified data for $[\mu\text{-}H\mathbf{1}^{NH}]^+$.

Proton Reduction Catalysis by $Fe_2(adt^{NH})(CO)_2(dppv)_2$.

In contrast to the behavior of the pdt complex, the voltammetry of $[t\text{-}H\mathbf{1}^{NH}]^+$ is strongly affected by relatively weak acids. Experiments employed $[Bu_4N]BAr^F_4$ as the electrolyte to maximize the equilibrium concentration of $[t\text{-}H\mathbf{1}^{NH}]^+$ vs its tautomer $[\mathbf{1}^{NH_2}]^+$. When $[t\text{-}H\mathbf{1}^{NH}]^+$ was generated *in situ* from $\mathbf{1}^{NH}$ and one equiv of $[H(OEt_2)_2]BAr^F_4$, the current for the $[t\text{-}H\mathbf{1}^{NH}]^{+/0}$ couple closely matched the current for the $[\mathbf{1}^{NH}]^{0/+}$ couple, indicating that both events correspond to one-electron couples. Whereas the couple $[\mathbf{2}H]^{+/0}$ is partially reversible, the $[t\text{-}H\mathbf{1}^{NH}]^{+/0}$ couple is completely irreversible (SI). Upon addition of $ClCH_2CO_2H$ to solutions of $\mathbf{1}^{NH}$, the reductive current at −1.64 V sharply increased and i_{pc} shifts to more positive potential (E_{cat} = −1.43 V), indicative of catalytic proton reduction (Figure 6).[35] A plot of i_c/i_p vs $[H^+]$ is linear over the range 50–400 equiv. The maximum $i_c/i_p \approx 69$ corresponds to a rate of 5000 s^{-1} (Figure 7). Gas chromatographic analysis showed that a 90% yield of hydrogen was produced by bulk electrolysis.

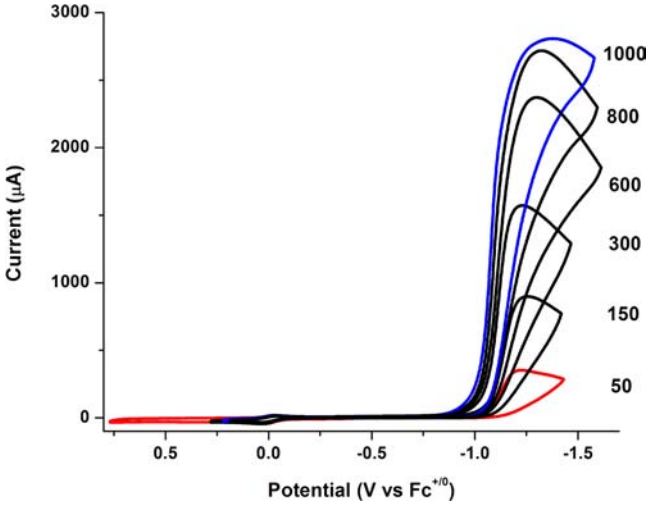

Figure 8. Cyclic voltammograms of a 0.5 mM solution of $\mathbf{1}^{NH}$ (0 °C, 0.125 M $[Bu_4N]BAr^F_4$, CH_2Cl_2, scan rate = 1.0 V/s, GC working electrode, Pt counter electrode, Ag wire pseudo reference electrode, Fc internal standard) recorded with increasing equivalents of CF_3CO_2H (shown to right of voltammograms).

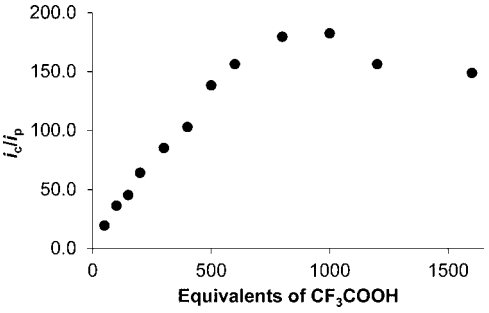

Figure 9. Dependence of i_c/i_p on equivalents of CF_3CO_2H added to a 0.5 mM solution of $\mathbf{1}^{NH}$ with $[Bu_4N]BAr^F_4$ as supporting electrolyte.

dx.doi.org/10.1021/ja309216v | J. Am. Chem. Soc. 2012, 134, 18843–18852

By the standards of synthetic catalysts, $[t\text{-H}\mathbf{1}^{\mathbf{NH}}]^+$ is a fast catalyst, but $[t\text{-H}\mathbf{1}^{\mathbf{NH_2}}]^{2+}$ appears to be even faster. Thus, in the presence of strong acids such as $HBF_4{\cdot}Et_2O$ or trifluoroacetic acid (TFA), a catalytic wave is observed at −1.22 V. Monitoring the current at −1.2 V, the variation of i_c/i_p vs [TFA] was found to be linear over 40−560 equiv. The maximum $i_c/i_p \approx 167$ corresponds to an estimated TOF of 58 000 s^{-1} (Figures 8 and 9).

Hydrogen evolution by electrolysis is typically subject to substantial isotope effects,[36] and this aspect was observed with $\mathbf{1}^{\mathbf{NH}}$. The dependence of the i_c/i_p vs $[ClCH_2CO_2D]$ is linear up to 60 equiv of acid and reaches a plateau at i_c/i_p = 18, which corresponds to a TOF of 420 s^{-1}. The rate decreased 10-fold compared to that exhibited in experiments that utilize $ClCH_2CO_2H$ (maximum i_c/i_p = 66, k = 4500 s^{-1}). Similarly, when CF_3CO_2D is substituted for CF_3CO_2H, k decreases by about 7-fold, with the maximum i_c/i_p = 106 and k = 6600 s^{-1}.

Electrocatalysis experiments were conducted with the bridging hydride $[\mu\text{-H}\mathbf{1}^{\mathbf{NH}}]^+$ also at 0 °C. At −1.8 V, the current increases with the addition of $ClCH_2CO_2H$. A plot of i_c/i_p vs $[H^+]$ is linear over the range 2−50 equiv of $ClCH_2CO_2H$ but begins to plateau at 60 equiv, corresponding to $i_c/i_p \approx 10$ (Figure 7). The catalytic rate is estimated as 20 s^{-1}. The μ-hydride operates at an overpotential of 0.9 V, which is 0.2−0.4 V higher than the overpotentials for the terminal species.

CONCLUSIONS

Hydrogen evolution by biomimetic diiron dithiolates is accelerated by the amine cofactor, to which the hydride ligand must be adjacent. The protonated derivatives of $\mathbf{1}^{\mathbf{NH}}$ and **2** exhibit very different catalytic properties, although the neutral complexes are almost indistinguishable spectroscopically. Thus, the adt and pdt ligands have comparable inductive effects, resulting in complexes of very similar thermodynamic properties.

The crystallographic analysis of $[t\text{-H}\mathbf{1}^{\mathbf{NH_2}}]^{2+}$ provides a unique insight into a probable intermediate in both the evolution and oxidation of hydrogen. The specific point of interest is the short distance between the hydride and the proton on the ammonium cofactor. The implied dihydrogen-bonding provides a snapshot of a step in the formation and scission of a dihydrogen molecule at the active site of the [FeFe]-H_2ase. An attractive $NH^{\delta+}$---$H^{\delta-}$ interaction may be relevant to the small separation between the first and second protonation constants, estimated at only 10^2 in CH_2Cl_2 solution. In comparison with $[t\text{-H}\mathbf{1}^{\mathbf{NH}}]^+$, $[t\text{-H}\mathbf{1}^{\mathbf{NH_2}}]^{2+}$ isomerizes to the μ-hydride more slowly, perhaps because this interaction stabilizes the terminal hydride.

The basicities of two sites—the terminal Fe center and the amine—are closely matched. In CH_2Cl_2 solution, Fe is more basic, but the equilibrium shifts in the presence of hydrogen-bond acceptors as demonstrated by the influence of $[Bu_4N]BF_4$ on this equilibrium. The lower basicity of a terminal Fe site vs the Fe−Fe bond is indicated by the conversion of $[\mathbf{1}^{\mathbf{NH_2}}]^+$ into $[\mu\text{-H}\mathbf{1}^{\mathbf{NH}}]^+$ under conditions where $[t\text{-H}\mathbf{1}^{\mathbf{NH}}]^+$ is undetectable. A sequence of three processes is invoked to explain the formation the μ-hydride under these conditions: (i) *N*-protonation, albeit unfavorable; (ii) tautomerization of ammonium species to the terminal hydride $[t\text{-H}\mathbf{1}^{\mathbf{NH}}]^+$; and (iii) isomerization of $[t\text{-H}\mathbf{1}^{\mathbf{NH}}]^+$ to $[\mu\text{-H}\mathbf{1}^{\mathbf{NH}}]^+$. The p$K_a$ of $[t\text{-H}\mathbf{1}^{\mathbf{NH}}]^+$ is estimated at 16, and the pK_a of $[\mu\text{-H}\mathbf{1}^{\mathbf{NH}}]^+$ is >18.6 (MeCN scale). Being a stronger acid, $[t\text{-H}\mathbf{1}^{\mathbf{NH}}]^+$ is more easily reduced than is $[\mu\text{-H}\mathbf{1}^{\mathbf{NH}}]^+$.

For both the pdt and adt derivatives, the terminal hydrides reduce at potentials that are 100−200 mV more positive than the corresponding bridging hydrides. The difference in reduction potentials between the isomeric hydrides is proposed to reflect differences in the localization of the reduction. In the case of the μ-hydride isomer, reduction is likely more delocalized between the two equivalent Fe centers.[38] When the hydride is bound to a single Fe atom, reduction likely occurs at the Fe center with no hydride ligand.[39] The crystallographic results presented above indicate how this reduction could induce the formation of a mixed valence dihydrogen complex (eq 1).

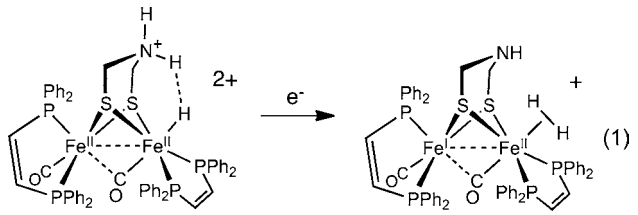

This scenario underscores the role of electron transfer, perhaps proton-coupled electron transfer (PCET),[40] in the hydrogen evolution reaction (HER, Scheme 3). Upon reduction, hydrogen evolution would produce the mixed valence derivative, analogous to the H_{ox} state of the enzyme.

In HER catalyzed by $[\mu\text{-H}\mathbf{1}^{\mathbf{NH}}]^+$, it is apparent that $\mathbf{1}^{\mathbf{NH}}$ is not regenerated. Otherwise, we would have observed increased rates during the electrolysis since $[t\text{-H}\mathbf{1}^{\mathbf{NH}}]^+$, which is such an

Scheme 3. Proposed Mechanism for Proton Reduction Catalyzed by $[t\text{-H}\mathbf{1}^{\mathbf{NH}}]^+$: Two Subcycles Are Shown for Strong and Weak Acids

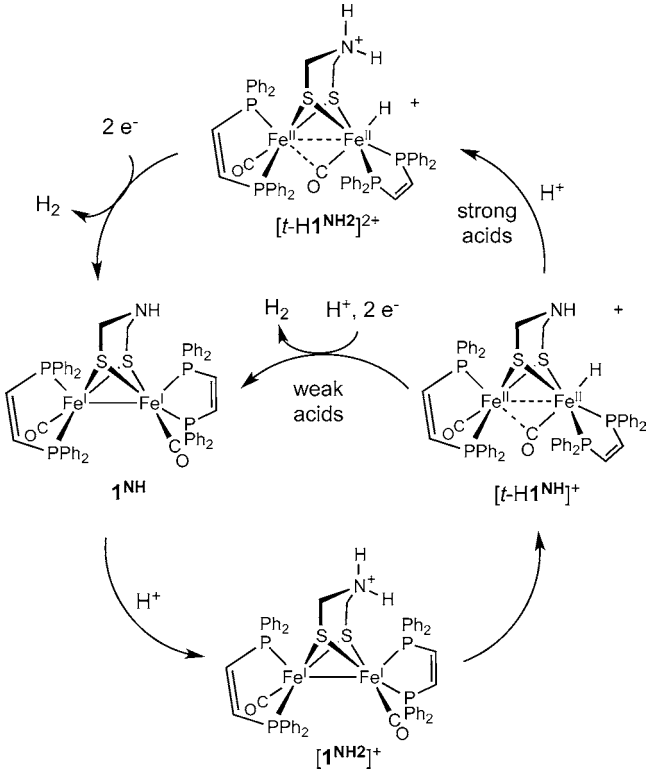

dx.doi.org/10.1021/ja309216v | J. Am. Chem. Soc. 2012, 134, 18843−18852

active catalyst, would be formed by protonation of $\mathbf{1}^{NH}$. We conclude therefore that the μ-hydride ligand in $[\mu\text{-H}\mathbf{1}^{NH}]^+$ is a spectator. A related mechanism was invoked by Talarmin for catalysis by $[Fe_2(pdt)(\mu\text{-H})(CO)_4(dppe)]^+$.[41]

Although the bioinspired complexes described in this report are highly active proton reduction catalysts,[42] challenges remain. These biomimetic catalysts suffer from relatively negative reduction potentials leading to high overpotentials.[5] One possible solution involves incorporation of redox-active center to mediate the PCET that is implicated for the breaking and making of the H−H bond.[40]

EXPERIMENTAL SECTION

Reactions were typically conducted using Schlenk techniques at room temperature. Most reagents were purchased from Aldrich and Strem. Solvents were HPLC-grade and dried by filtration through activated alumina or distilled under nitrogen over an appropriate drying agent. $HBF_4{\cdot}Et_2O$ (Sigma-Aldrich) was supplied as 51−57% HBF_4 in Et_2O (6.91−7.71 M). $[H(OEt_2)_2]BAr^F{}_4$ was prepared by literature methods.[43] $[Bu_4N]PF_6$ was purchased from GFS Chemicals and was recrystallized multiple times by extraction into acetone followed by precipitation by ethanol. ^{1}H NMR spectra (500 and 400 MHz) are referenced to residual solvent referenced to TMS. $^{31}P\{^1H\}$ NMR spectra (202 and 161 MHz) are referenced to external 85% H_3PO_4. FT-IR spectra were recorded on a Perkin-Elmer 100 FT-IR spectrometer. CF_3CO_2D was purchased from Sigma-Aldrich. CCl_2HCO_2D was prepared by treating the acid in D_2O.

$Fe_2(adt^{NH})(CO)_4(dppv)$. A solution of $Fe_2(adt^{NH})(CO)_6$[44] (175 mg, 0.45 mmol) and dppv (179 mg, 0.45 mmol) in 15 mL of toluene was treated with a solution of anhydrous Me_3NO (34 mg, 0.45 mmol) in ca. 5 mL of MeCN. Bubbles appeared, and the reaction mixture darkened. After heating of the mixture at reflux for 5 h, the FT-IR spectrum indicated complete conversion to product. Solvent was removed under vacuum, and the product was extracted into 5 mL of CH_2Cl_2. Addition of 50 mL of hexane precipitated the product. Yield: 0.260 g (80%). FT-IR, ^{1}H NMR, and ^{31}P NMR results matched reported values.[24]

$Fe_2(adt^{NH})(CO)_2(dppv)_2$ ($\mathbf{1}^{NH}$). A solution of $Fe_2(adt^{NH})(CO)_4(dppv)$ (400 mg, 0.55 mmol) in 40 mL of toluene was treated with dppv (872 mg, 2.2 mmol) in 10 mL of toluene. The mixture was irradiated at 365 nm until the conversion was complete (∼24 h) as indicated by IR spectroscopy. The solvent was removed in vacuum, and the product was extracted into ∼3 mL of toluene. The green product precipitated upon addition of methanol to the toluene extract. The product was then re-extracted into ∼2 mL of CH_2Cl_2, and the product precipitated as an olive-green powder upon the addition of 100 mL of hexanes. Yield: 150 mg (26%). ^{1}H NMR (500 MHz, CD_2Cl_2): δ 8.1−7.0 (m, 40H, $P(C_6H_5)_2$), 2.3 (s, 4H, $(SCH_2)_2NH$). ^{31}P NMR (CD_2Cl_2, 20 °C): δ 92. ^{31}P NMR (CD_2Cl_2, −70 °C): δ 102.6, 93.4, 92.2, 88.6. FT-IR (CH_2Cl_2): ν_{CO} = 1888, 1868 cm^{-1}. Anal. Calcd for $C_{56}H_{49}Fe_2O_2NP_4S_2{\cdot}CH_2Cl_2{\cdot}CH_3OH$ (found): C, 58.8 (58.15); H, 4.68 (4.63); N 1.18 (1.10). Diffraction-quality crystals were grown at −20 °C from a CH_2Cl_2 solution of **1** layered with pentane.

$[HFe_2(adt^{NH})(CO)_2(dppv)_2]BAr^F{}_4$ ($[t\text{-H}\mathbf{1}^{NH}]BAr^F{}_4$), $[Fe_2(adt^{NH})(CO)_2(dppv)_2]BAr^F{}_4$ ($[\mu\text{-H}\mathbf{1}^{NH}]BAr^F{}_4$), and $[Fe_2(adt^{NH_2})(\mu\text{-H})(CO)_2(dppv)_2](BAr^F{}_4)_2$ ($[\mu\text{-H}\mathbf{1}^{NH_2}](BAr^F{}_4)_2$). Into a liquid nitrogen-cooled J. Young NMR tube, ∼0.5 mL of CD_2Cl_2 was distilled and frozen onto a mixture of $\mathbf{1}^{NH}$ (5 mg, 0.005 mmol) and $[H(OEt_2)_2]BAr^F{}_4$ (5 mg, 0.005 mmol). The sample was then gently warmed to near −78 °C before analysis by NMR spectroscopy. ^{1}H NMR (600 MHz, CD_2Cl_2, −80 °C): δ −4.2 (t, Fe−H, $^2J_{PH}$ = 73 Hz). $^{31}P\{^1H\}$ NMR (242 MHz, CD_2Cl_2, −40 °C): δ 103.2 (s), 94.5 (s), 84.0 (s), 75.1 (s). Selective ^{31}P decoupling of the ^{1}H NMR verified that only the signals at δ 94 and 84 were coupled to the hydride, and presumably these correspond to dibasal phosphines attached to the FeH center. At the sample temperature of −10 °C, a triplet of triplets at δ −14.8 (Fe-μH, J_{PH} = 25, 5 Hz) appears in the ^{1}H NMR spectrum, and singlets at δ 91.0 and 90.8 appear in the ^{31}P NMR spectrum, which are assigned to *sym*-$[\mu\text{-H}\mathbf{1}^{NH}]BAr^F{}_4$. Upon warming of the sample to 20 °C, signals corresponding to $[t\text{-H}\mathbf{1}^{NH}]BAr^F{}_4$ disappear, and only *sym*-$[\mu\text{-H}\mathbf{1}^{NH}]BAr^F{}_4$ is observed. After ∼10 min at 20 °C, an additional ^{1}H NMR multiplet at δ −13.7 appears, and four ^{31}P NMR singlets appear at δ 88.2, 85.7, 82.7, and 77.3, which are assigned to *unsym*-$[\mu\text{-H}\mathbf{1}^{NH}]BAr^F{}_4$. After ∼12 h at room temperature, the ratio of the *sym*:*unsym* isomers is 1:5.

Upon addition of a second equivalent of $[H(OEt_2)_2]BAr^F{}_4$ (5 mg, 0.005 mmol) to the solution, the ^{1}H NMR spectrum showed a triplet of triplets at δ −15.5 (Fe-μH, J_{PH} = 25, 5 Hz) assigned to *sym*-$[\mu\text{-H}\mathbf{1}^{NH_2}](BAr^F{}_4)_2$ and a multiplet at δ −14.3 assigned to *unsym*-$[\mu\text{-H}\mathbf{1}^{NH_2}](BAr^F{}_4)_2$. Additionally, in the ^{31}P NMR spectrum, signals are observed at δ 91.3 and 88.7 (*sym*-$[\mu\text{-H}\mathbf{1}^{NH_2}](BAr^F{}_4)_2$) and at δ 92.3, 86.0, 82.4, and 79.0 (*unsym*-$[\mu\text{-H}\mathbf{1}^{NH_2}](BAr^F{}_4)_2$). The two isomers are present in a ratio of 5:1 *sym*:*unsym*. An IR spectrum of the CD_2Cl_2 solution features bands at 1967 and 1985 cm^{-1}.

$[t\text{-HFe}_2(adt^{NH_2})(CO)_2(dppv)_2](BAr^F{}_4)_2$ ($[t\text{-H}\mathbf{1}^{NH_2}](BAr^F{}_4)_2$). Into a liquid nitrogen-cooled J. Young NMR tube, ∼0.5 mL of CD_2Cl_2 was distilled onto a mixture of $\mathbf{1}^{NH}$ (5 mg, 0.005 mmol) and $[H(OEt_2)_2]BAr^F{}_4$ (10 mg, 0.010 mmol). The sample was then gently warmed to near −78 °C before analysis by low-temperature NMR spectroscopy. High-field ^{1}H NMR (600 MHz, CD_2Cl_2, −40 °C): δ −4.95 (t, Fe−H, $^2J_{PH}$ = 72 Hz). $^{31}P\{^1H\}$ NMR (242 MHz, CD_2Cl_2, −40 °C): δ 98 (s), 89 (s), 76 (s), 74 (s). Decoupling experiments verified that the high-field ^{1}H NMR signal is coupled to the ^{31}P NMR signals at δ 89 and 74.

Crystallization of $[t\text{-HFe}_2(adt^{NH_2})(CO)_2(dppv)_2](BF_4)_2$. Crystals were obtained by treating a CH_2Cl_2 solution of $\mathbf{1}^{NH}$, at 0 °C, with 2 equiv of $HBF_4{\cdot}Et_2O$ and layering with cold pentane. Storage at −20 °C gave dark brown crystals.

$[Fe_2(adt^{NH})(\mu\text{-H})(CO)_2(dppv)_2]BAr^F{}_4$ ($[\mu\text{-H}\mathbf{1}^{NH}]BAr^F{}_4$). A 10 mL solution of $\mathbf{1}^{NH}$ (35 mg, 0.03 mmol) in CH_2Cl_2 was treated with a 5 mL solution of $[H(OEt_2)_2]BAr^F{}_4$ (33 mg, 0.03 mmol) in CH_2Cl_2. Within 5 min, the solution color changed from green to brown. After being stirred at room temperature for 22 h, the solution was concentrated to ∼5 mL, and the brown product was precipitated with addition of 20 mL of Et_2O. IR (CH_2Cl_2): ν_{CO} = 1948, 1969 (sh) cm^{-1}. ^{1}H and ^{31}P NMR data match those described above. Anal. Calcd for $C_9H_{62}BF_{24}Fe_2NO_2P_4S_2{\cdot}2CH_2Cl_2{\cdot}C_4H_{10}O$ (found): C, 51.89 (52.19); H, 3.52 (3.13); N 0.64 (0.76).

Protonation of $Fe_2(adt^{NH})(CO)_2(dppv)_2$ with 1.5 equiv of $[H(OEt_2)_2]BAr^F{}_4$. Into a liquid nitrogen-cooled J. Young NMR tube, CD_2Cl_2 was distilled onto a mixture of $\mathbf{1}^{NH}$ (5 mg, 0.005 mmol) and $[H(OEt_2)_2]BAr^F{}_4$ (7.5 mg, 0.0075 mmol). The sample was then gently warmed to near −78 °C before analysis by low-temperature NMR spectroscopy. High-field ^{1}H NMR (600 MHz, CD_2Cl_2, −40 °C): δ −4.95 (Fe-*H*, $^2J_{PH}$ = 72 Hz), −4.2 (Fe−H, $^{x2}J_{PH}$ = 73 Hz).

Effect of $[Bu_4N]BF_4$ on Equilibrium between Tautomers $[t\text{-H}\mathbf{1}^{NH}]^+$ and $[\mathbf{1}^{NH_2}]^+$. A 7 mM solution of $[t\text{-H}\mathbf{1}^{NH}]BAr^F{}_4$ was prepared by dissolving $\mathbf{1}^{NH}$ (15 mg, 0.014 mmol) and $[H(Et_2O)_2]BAr^F{}_4$ (15 mg, 0.014 mmol) in 2 mL of CH_2Cl_2, which had been precooled to −78 °C. Aliquots of a 0.6 M $[Bu_4N]BF_4$ solution were added to the solution. After each addition, 0.1 mL aliquots were removed and immediately analyzed by IR spectroscopy.

$[t\text{-HFe}_2(pdt)(\mu\text{-CO})(CO)(dppv)_2]BF_4$ ($[t\text{-H2}]BF_4$). A dark green solution of **2** (205 mg, 0.192 mmol) in 5 mL of CH_2Cl_2 was treated at −40 °C with $HBF_4{\cdot}Et_2O$ (5 mL 0.04 M, 0.2 mmol). The resulting darker green solution was then diluted with 100 mL of cold (−78 °C) Et_2O, producing a green precipitate. The precipitate was collected by filtration at −78 °C, washed with 2 × 10 mL of Et_2O, and dried under vacuum prior to storage at −30 °C. Yield: 140 mg (63%). ^{1}H NMR (500 MHz, CD_2Cl_2): δ −3.5 (t, Fe−H, $^2J_{PH}$ = 76 Hz). $^{31}P\{^1H\}$ NMR (202 MHz, CD_2Cl_2): δ 99 (s), 91 (s), 86 (s), 68 (s). Selective ^{31}P-decoupled ^{1}H NMR verified that the signals at δ 91 and 86 were coupled to the hydride signal. FT-IR (CH_2Cl_2, cm^{-1}): ν_{CO} = 1965, 1905, 1988.

$[Fe_2(pdt)(\mu\text{-H})(CO)_2(dppv)_2]PF_6$ ($[\mu\text{-H2}]PF_6$). In a 250 mL Schlenk flask, a dark green solution of **1** (200 mg, 0.187 mmol) in 5 mL of CH_2Cl_2 was treated at room temperature with a solution of 2.0

dx.doi.org/10.1021/ja309216v | J. Am. Chem. Soc. 2012, 134, 18843−18852

M HCl in Et_2O (0.2 mL, 0.2 mmol). Solvent was removed under vacuum, and the solid was redissolved in MeOH. The product was precipitated as its PF_6^- salt by addition of ca. 5 mL of a saturated aqueous solution of NH_4PF_6. The brownish precipitate was then transferred anaerobically onto a Celite plug in a chromatography column, where it was washed with 6 × 30 mL of H_2O and 6 × 30 mL of Et_2O. The product was then extracted off the Celite with CH_2Cl_2, and solvent was removed under vacuum. The product was dissolved with 5 mL of CH_2Cl_2, which was diluted with 5 mL of MeOH. Addition of 50 mL of hexane to this solution yielded a brown powder, which was collected by filtration and dried. Yield: 170 mg (75%). High-field ^{1}H NMR (500 MHz, CD_2Cl_2): δ −14.5 (dddd, μ-H, J_{PH1} = 24, J_{PH2} = 19, J_{PH3} = 10 Hz), −15.6 (tt, μ-H, J_{PH1} = 24, J_{PH2} = 6 Hz). ^{31}P{^{1}H} NMR (202 MHz, CD_2Cl_2): δ 89.6 (s), 89.6 (s), δ 76.7 (s), 82.8 (s), 84.2 (s), 87.8 (s). FT-IR (CH_2Cl_2, cm^{-1}): ν_{CO} = 1963, 1951. Anal. Calcd for $C_{57}H_{51}F_6Fe_2O_2P_5S_2$ (found): C, 56.45 (56.28); H, 4.24 (4.28); Fe 9.21 (8.79).

Electrochemistry. Electrochemical experiments were carried out on CH Instruments model 600D series electrochemical analyzer or a BAS-100 electrochemical analyzer. Cyclic voltammetry experiments were conducted using a 10-mL one-compartment glass cell with a tight-fitting Teflon top. The working electrode was a glassy carbon (GC) disk (diameter = 3.00 mm). A Ag wire was used as a quasi-reference electrode, and the counter electrode was a Pt wire. Ferrocene was added as an internal reference, and each cyclic voltammogram (CV) was referenced to this $Fc^{0/+}$ couple = 0.00 V. *iR* compensation was applied to all measurements using the CH Instruments or BAS software. Cell resistance was determined prior to each scan, and the correction applied to the subsequently collected CV. During prolonged experiments, additional solvent was added to compensate for evaporative loss. Between scans, the solution was purged briefly with N_2, and the working GC electrode was removed and polished. The duration of typical electrochemical titrations was 30 min. For all experiments, the electrolyte solution was prepared and sparged in the cell, which was fitted with electrodes. A CV of the electrolyte was collected prior to the addition of Fe_2 compound, in order to check the purity of the electrolyte. The diiron compound was then dissolved in the electrolyte solution and transferred to the cell.

Due to their tendency to isomerize above 0 °C, [*t*-H**1**^{NH}]$^+$, [*t*-H**1**^{NH_2}]$^{2+}$, and [*t*-H**2**]$^+$ were generated *in situ*. The corresponding bridging hydrides were isolated as their BF_4^- salts prior to electrochemical experiments. All electrochemical experiments were conducted at 0 °C.

■ ASSOCIATED CONTENT

Ⓢ Supporting Information

Results from NMR, IR spectra, X-ray crystallographic, and electrochemical analyses. This material is available free of charge via the Internet at http://pubs.acs.org.

■ AUTHOR INFORMATION

Corresponding Author

rauchfuz@illinois.edu

Notes

The authors declare no competing financial interest.

■ ACKNOWLEDGMENTS

This work was supported by the National Institutes of Health (Grant GM61153). This work was also supported in part by the ANSER Center, an Energy Frontier Research Center funded by the U.S. Department of Energy, Office of Science, Office of Basic Energy Sciences, under Award Number DE-SC0001059. We thank Danielle Gray for collecting crystallographic data.

■ REFERENCES

(1) Cammack, R.; Frey, M.; Robson, R. *Hydrogen as a Fuel: Learning from Nature*; Taylor & Francis: London, 2001.

(2) Fontecilla-Camps, J. C.; Amara, P.; Cavazza, C.; Nicolet, Y.; Volbeda, A. *Nature* **2009**, *460*, 814.

(3) Tard, C.; Pickett, C. J. *Chem. Rev.* **2009**, *109*, 2245.

(4) Rakowski DuBois, M.; DuBois, D. L. *Acc. Chem. Res.* **2009**, *42*, 1974. *Catalysis without Precious Metals*; Bullock, R. M., Ed.; Wiley-VCH: Weinheim, 2010.

(5) Fontecilla-Camps, J. C.; Volbeda, A.; Cavazza, C.; Nicolet, Y. *Chem. Rev.* **2007**, *107*, 4273.

(6) Peters, J. W.; Lanzilotta, W. N.; Lemon, B. J.; Seefeldt, L. C. *Science* **1998**, *282*, 1853.

(7) Frey, M. *ChemBioChem* **2002**, *3*, 153.

(8) Silakov, A.; Wenk, B.; Reijerse, E.; Lubitz, W. *Phys. Chem. Chem. Phys.* **2009**, *11*, 6592.

(9) Tschierlei, S.; Ott, S.; Lomoth, R. *Energy Environ. Sci.* **2011**, *4*, 2340.

(10) Nametkin, N. S.; Tyurin, V. D.; Kukina, M. A. *Russ. Chem. Rev.* **1986**, *55*, 439. Linford, L.; Raubenheimer, H. G. *Adv. Organomet. Chem.* **1991**, *32*, 1.

(11) Schmidt, M.; Contakes, S. M.; Rauchfuss, T. B. *J. Am. Chem. Soc.* **1999**, *121*, 9736. Le Cloirec, A.; Davies, S. C.; Evans, D. J.; Hughes, D. L.; Pickett, C. J.; Best, S. P.; Borg, S. *Chem Commun.* **1999**, 2285. Lyon, E. J.; Georgakaki, I. P.; Reibenspies, J. H.; Darensbourg, M. Y. *Angew. Chem., Int. Ed.* **1999**, *38*, 3178. Gloaguen, F.; Lawrence, J. D.; Schmidt, M.; Wilson, S. R.; Rauchfuss, T. B. *J. Am. Chem. Soc.* **2001**, *123*, 12518.

(12) Gloaguen, F.; Rauchfuss, T. B. *Chem. Soc. Rev.* **2009**, *38*, 100.

(13) Barton, B. E.; Olsen, M. T.; Rauchfuss, T. B. *J. Am. Chem. Soc.* **2008**, *130*, 16834.

(14) Nakazawa, H.; Itazaki, M. *Top. Organomet. Chem.* **2011**, *33*, 27.

(15) Matthews, S. L.; Heinekey, D. M. *Inorg. Chem.* **2010**, *49*, 9746.

(16) Bruschi, M.; Greco, C.; Kaukonen, M.; Fantucci, P.; Ryde, U.; De Gioia, L. *Angew. Chem., Int. Ed.* **2009**, *48*, 3503.

(17) Ezzaher, S.; Capon, J.-F.; Gloaguen, F.; Pétillon, F. Y.; Schollhammer, P.; Talarmin, J.; Pichon, R.; Kervarec, N. *Inorg. Chem.* **2007**, *46*, 3426.

(18) Barton, B. E.; Zampella, G.; Justice, A. K.; De Gioia, L.; Rauchfuss, T. B.; Wilson, S. R. *Dalton Trans.* **2010**, *39*, 3011.

(19) Barton, B. E.; Rauchfuss, T. B. *Inorg. Chem.* **2008**, *47*, 2261.

(20) van der Vlugt, J. I.; Rauchfuss, T. B.; Whaley, C. M.; Wilson, S. R. *J. Am. Chem. Soc.* **2005**, *127*, 16012.

(21) Singleton, M. L.; Jenkins, R. M.; Klemashevich, C. L.; Darensbourg, M. Y. *C. R. Chim.* **2008**, *11*, 861.

(22) Winter, A.; Zsolnai, L.; Huttner, G. *Z. Naturforsch.* **1982**, *37b*, 1430.

(23) Lambert, J. B.; Featherman, S. I. *Chem. Rev.* **1975**, *75*, 611.

(24) Justice, A. K.; Zampella, G.; De Gioia, L.; Rauchfuss, T. B.; van der Vlugt, J. I.; Wilson, S. R. *Inorg. Chem.* **2007**, *46*, 1655.

(25) Ott, S.; Kritikos, M.; Åkermark, B.; Sun, L.; Lomoth, R. *Angew. Chem., Int. Ed.* **2004**, *43*, 1006. Schwartz, L.; Eilers, G.; Eriksson, L.; Gogoll, A.; Lomoth, R.; Ott, S. *Chem. Commun.* **2006**, 520.

(26) Lawrence, J. D.; Li, H.; Rauchfuss, T. B.; Bénard, M.; Rohmer, M.-M. *Angew Chem., Int. Ed.* **2001**, *40*, 1768.

(27) Basallote, M. G.; Besora, M.; Castillo, C. E.; Fernández-Trujillo, M. J.; Lledós, A.; Maseras, F.; Máñez, M. A. *J. Am. Chem. Soc.* **2007**, *129*, 6608.

(28) Das, P.; Capon, J.-F.; Gloaguen, F.; Pétillon, F. Y.; Schollhammer, P.; Talarmin, J.; Muir, K. W. *Inorg. Chem.* **2004**, *43*, 8203.

(29) Olsen, M. T.; Bruschi, M.; De Gioia, L.; Rauchfuss, T. B.; Wilson, S. R. *J. Am. Chem. Soc.* **2008**, *130*, 12021.

(30) Ho, N. N.; Bau, R.; Mason, S. A. *J. Organomet. Chem.* **2003**, *676*, 85.

(31) Custelcean, R.; Jackson, J. E. *Chem. Rev.* **2001**, *101*, 1963.

(32) Izutsu, K. *Acid-Base Dissociation Constants in Dipolar Aprotic Solvents*; Blackwell Scientific Publications: Oxford, U.K., 1990.

(33) Felton, G. A. N.; Mebi, C. A.; Petro, B. J.; Vannucci, A. K.; Evans, D. H.; Glass, R. S.; Lichtenberger, D. L. *J. Organomet. Chem.* **2009**, *694*, 2681.

(34) Justice, A. K.; De Gioia, L.; Nilges, M. J.; Rauchfuss, T. B.; Wilson, S. R.; Zampella, G. *Inorg. Chem.* **2008**, *47*, 7405.
(35) Felton, G. A. N.; Glass, R. S.; Lichtenberger, D. L.; Evans, D. H. *Inorg. Chem.* **2006**, *45*, 9181.
(36) Miller, M. A.; Carey, A. A. In *Ullmann's Encyclopedia of Industrial Chemistry*; Wiley-VCH: Weinheim, 2000.
(37) Fourmond, V.; Jacques, P.-A.; Fontecave, M.; Artero, V. *Inorg. Chem.* **2010**, *49*, 10338.
(38) Jablonskya, A.; Wright, J. A.; Fairhurst, S. A.; Peck, J. N. T.; Ibrahim, S. K.; Oganesyan, V. S.; Pickett, C. J. *J. Am. Chem. Soc.* **2011**, *133*, 18606.
(39) Lever, A. B. P. *Inorg. Chem.* **1990**, *29*, 1271.
(40) Camara, J. M.; Rauchfuss, T. B. *J. Am. Chem. Soc.* **2011**, *133*, 8098. Camara, J. M.; Rauchfuss, T. B. *Nat. Chem.* **2012**, *4*, 26.
(41) Ezzaher, S.; Capon, J.-F.; Dumontet, N.; Gloaguen, F.; Pétillon, F. Y.; Schollhammer, P.; Talarmin, J. *J. Electroanal. Chem.* **2009**, *626*, 161.
(42) Helm, M. L.; Stewart, M. P.; Bullock, R. M.; Rakowski DuBois, M.; DuBois, D. L. *Science* **2011**, *333*, 863. Cheah, M. H.; Tard, C.; Borg, S. J.; Liu, X.; Ibrahim, S. K.; Pickett, C. J.; Best, S. P. *J. Am. Chem. Soc.* **2007**, *129*, 11085.
(43) Brookhart, M.; Grant, B.; Volpe, A. F. *Organometallics* **1992**, *11*, 3920.
(44) Zaffaroni, R.; Rauchfuss, T. B.; Gray, D. L.; De Gioia, L.; Zampella, G. *J. Am. Chem. Soc.* **2012**, DOI: 10.1021/ja3094394.